Journal Pre-proof

Ti_3C_2 MXene-based Schottky Photocathode for Enhanced Photoelectrochemical Sensing

Cui Ye, Zhen Wu, Keyi Ma, Zhuohao Xia, Jun Pan, Minqiang Wang, Changhui Ye

PII: S0925-8388(20)34151-7

DOI: https://doi.org/10.1016/j.jallcom.2020.157787

Reference: JALCOM 157787

To appear in: *Journal of Alloys and Compounds*

Received Date: 17 June 2020

Revised Date: 27 October 2020

Accepted Date: 29 October 2020

Please cite this article as: C. Ye, Z. Wu, K. Ma, Z. Xia, J. Pan, M. Wang, C. Ye, Ti_3C_2 MXene-based Schottky Photocathode for Enhanced Photoelectrochemical Sensing, *Journal of Alloys and Compounds*, https://doi.org/10.1016/j.jallcom.2020.157787.

Ti_3C_2 MXene-based Schottky Photocathode for Enhanced Photoelectrochemical Sensing

Cui Ye,[*,a] Zhen Wu,[a] Keyi Ma,[a] Zhuohao Xia,[a] Jun Pan,[*,a] Minqiang Wang,[*,b] Changhui Ye[a]

[a] College of Materials Science and Engineering, Zhejiang University of Technology, Hangzhou 310014, China

[b] Division of Engineering and Applied Science, California Institute of Technology, Pasadena, California 91125, United States

Abstract

Nanomaterials are vital to the realization of photoelectrochemical (PEC) sensing platfrom that provides the sensitive detection and quantification of low-abundance biological samples. Here, this work reports a Schottky junction-based BiOI/Ti_3C_2 heterostructure, used as a photocathode for PEC bioanalysis. Specially, we realize *in situ* growth of flower-like BiOI on 2D intrinsically negatively charged Ti_3C_2 MXene nanosheet that endows BiOI/Ti_3C_2 heterostructure with admirably combined merits, noting in particular the generation of built-in electric field and the decrease of contact resistance between BiOI and Ti_3C_2. Under the visible light irradiation, the BiOI/Ti_3C_2 heterostructure-modified PEC platform displays superior cathodic photocurrent signal, while PEC response cuts down with the presence of L-Cysteine (L-Cys) as a representative analyte owing to the metal-S bond formation. The “signal-off” PEC sensing strategy shows good performance in terms of sensitivity, limit of detection (LOD, 0.005 nM) and stability. This research reveals the great potentials of MXene-based heterostructure in the application field of PEC sensor establishment.

Keywords: Ti_3C_2 MXene; Photoelectrochemical Sensing, Schottky Junction; L-Cysteine

1. Introduction

Photoelectrochemical (PEC) sensing has been a rapidly evolving analytical technique for trace or ultratrace detection towards diverse biomolecular in complex samples, since the technique is of considerate merits of low background signal, high sensitivity, and simple operating conditions [1-3]. Potential photoelectrode candidates should possess highly valid light harvesting, suitable analytes interfacing, efficient PEC signal response, and stable signal transduction to exploit ideal PEC sensing platform [4-6]. Up to now, plentiful efforts are focused on developing photoactive materials to obtain desirable photoelectrode, such as TiO_2-based or quantum dots-based nanomaterials, as well as porphyrin and its derivatives [7,8]. As a matter of fact, advanced heterostructure of various components that formulates Schottky junction can be conducive to carrier generation, and transfer, thus acquiring astonishing performance [9,10].

Recently, research on Ti_3C_2 MXene is booming, firstly reported by Gogotsi and his group in 2011 [11]. As a new family of 2D transition metal carbides/carbonitrides/nitrides, MXene is obtained by selective etching away A layers from $M_{n+1}AX_n$ (MAX) phases (M represents transition metal, A represents group IIIA/IVA element, X represents C/N element and n = 1–3). Ti_3C_2, one of the most widely used MXene, possesses lots of superior merits including electronic conductivity, mechanical property, huge surface area, especially compatibility with other nanomaterials. The mentioned merits make Ti_3C_2 MXene be widely used in electrocatalysis [12], energy storage batteries [13], electrochemical sensor [14,15] and so on, yet Ti_3C_2 MXene-based photoelectrochemical (PEC) sensing has seldom been exploited so far. It is worth noting that MXene, particularly OH-functionalized Ti_3C_2, can be efficiently conductive to separate and transmit the photogenerated carriers in a Ti_3C_2/semiconductor heterostructure, since there is difference between valance band and Fermi levels (EF) to generate Schottky junction, and then give rise to the built-in electric field between Ti_3C_2 and photoactive materials such as semiconductor [16,17]. Besides, integrated with the unique properties of intrinsically negatively charged

surfaces and active OH-Ti sites on accordion-like multilayer architecture, as well as the Schottky barrier near to zero by first principle calculation [18], Ti_3C_2-based hybrid composite is potentially motivated to fabricate functional PEC loading platform, thus exploiting it in PEC sensing domain.

Bismuth oxyiodide (BiOI), a typical p-type semiconductor with a narrow band gap (about 1.8 eV), has been widely used as an economical and promising visible-light-driven (VLD) photocathode materials [19,20]. Since pure BiOI suffers from quick recombination of photogenerated electron-hole pairs and poor conductivity, engineering BiOI by compounding with Ti_3C_2 is undoubtedly logical. Differing from previous widely reported photoactive materials, BiOI/Ti_3C_2 heterostructure not only equipped with efficient photoconversion efficiency, but also diminish the contact resistance due to their combined properties. In this respect, we propose the novel BiOI/Ti_3C_2 heterostructure regarding as photocathode to construct PEC sensing platform. And we adopt a typical thiol-containing amino L-Cysteine (L-Cys) to explore the PEC sensing performance, which is broadly used in clinical diagnoses because it is concerned with lots of syndromes such as hypoglycemic brain and liver damage, skin lesions, as well as hair depigmentation, and can regulate the function of a biological system [21-23].

Herein, we develop BiOI/Ti_3C_2 heterostructure-based photocathode using L-Cys as a model molecule to demonstrate the PEC sensing strategy. Detailedly, 2D Ti_3C_2 nanosheet is obtained by exfoliating bulk Ti_3AlC_2 in a mixture of LiF and HCl, and is taken to mediates the *in situ* BiOI generation on account of the admirable adsorption affinity to metal ions, which endows BiOI/Ti_3C_2 heterostructure with Schottky junction. In the PEC sensing strategy, enormous cathodic photocurrent derived from VLD BiOI/Ti_3C_2 heterostructure was generated, and obvious decrease of PEC response was observed because of interaction of metal-S bond [24], thus realizing the cathodic “signal-off” pattern-based PEC selective sensing of L-Cys (Scheme 1). This work is benefit to inspire more rational designs of Ti_3C_2-based heterostructure with Schottky junction for further diverse establishment of PEC sensing platform.

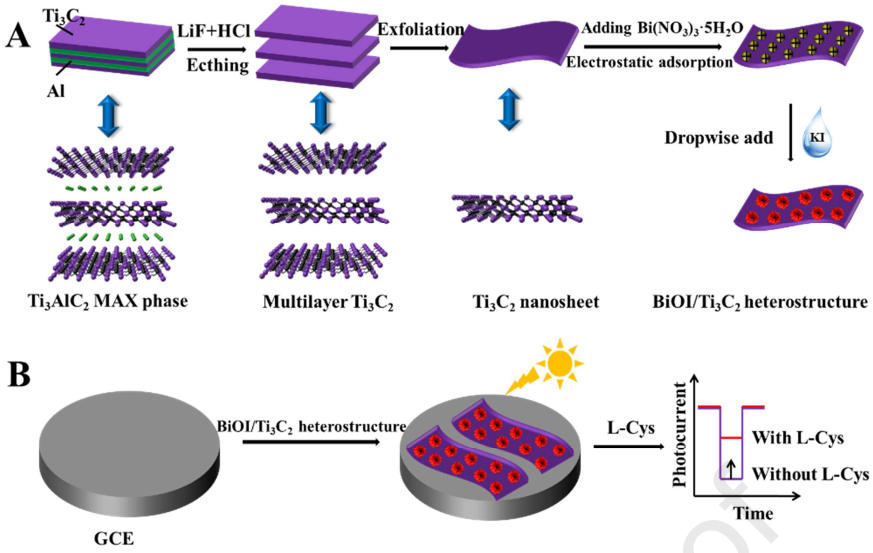

Scheme 1. (A) Synthesis of BiOI/Ti_3C_2 heterostructure; (B) schematic illustration of fabricating PEC sensing L-Cys detection.

2. Experimental

2.1 Synthesis of Ti_3C_2 nanosheets.

Ti_3C_2 nanosheets were prepared *via* a previously reported method [11,25]. Briefly, LiF (0.5 g) was dissolved in HCl (9 M, 10 mL) under stirring at room temperature to obtain the LiF/HCl solution. Then, Ti_3AlC_2 (MAX phase, 0.5 g) was slowly added to the above LiF/HCl solution within 5 min. The suspension was stirred at 35 °C for 24 h. The product was washed with ultrapure water under centrifugation (3500 rpm, 5 min) until the pH value of the filtrate reached 6.0. The precipitate was taken out and added to ultrapure water to obtain the Ti_3C_2 suspension (10 mg mL^{-1}, 30 mL). After that, the Ti_3C_2 suspension was ultrasonicated for 30 min under the nitrogen atmosphere. Finally, the supernatant of Ti_3C_2 nanosheets was gathered *via* centrifugation at 7500 rpm for 20 min.

2.2 Preparation of BiOI/Ti_3C_2 heterostructure.

For synthesis of BiOI/Ti_3C_2 heterostructure, ($Bi(NO_3)_3·5H_2O$) (0.25 mmol) was added to the supernatant of Ti_3C_2 nanosheets (0.5 mg mL^{-1}, 5 mL) and stirred for 30 min to obtain a homogeneous solution (referred to as Solution A). Meanwhile, KI (0.25 mmol) was dissolved in ethylene glycol (5 mL) (referred to as Solution B). Then,

Solution B was added dropwise to Solution A under stirred constantly. The resultant product obtained after washing several times with ultrapure water and drying under vacuum at 80 °C for 6 hours. For comparison, the pure BiOI was prepared in the absence of Ti_3C_2 nanosheets under the same condition.

2.3 Preparation of PEC sensing platform.

A glassy carbon electrode (GCE) was used to study the PEC performance of BiOI/Ti_3C_2 heterostructure. Prior to modification, the GCE surface was polished with alumina slurry of 0.3 μm and 0.05 μm and sonicated in ethanol and ultrapure water. Then, BiOI/Ti_3C_2 heterostructure was sonicated in ultrapure water for 1 min to obtain uniformly distributed suspension with a concentration of 2 mg mL^{-1}. 10 μL of the above solution was dripped onto GCE and evaporated at room temperature, the modified photoelectrode was referred to as BiOI/Ti_3C_2/GCE. Furthermore, the BiOI/Ti_3C_2/GCE was incubated with L-Cys (10 μL) for 30 min, followed by washing and drying. Finally, the BiOI/Ti_3C_2/GCE was stored in a refrigerator for further studies.

2.4 PEC detection for L-Cys.

The PEC experiments were recorded on a CHI760 E electrochemical work station using a three-electrode system with the modified GCE as the working electrode, platinum wire as the counter electrode, and Ag/AgCl as the reference electrode. For L-Cys monitoring, the photocurrent response of the BiOI/Ti_3C_2/GCE incubated with various concentrations of L-Cys was measured in 0.1 M phosphate buffer (PH 7.4) by applying a bias potential of -0.2 V under visible light irradiation (300 W Xenon lamp) at room temperature.

3. Results and discussion

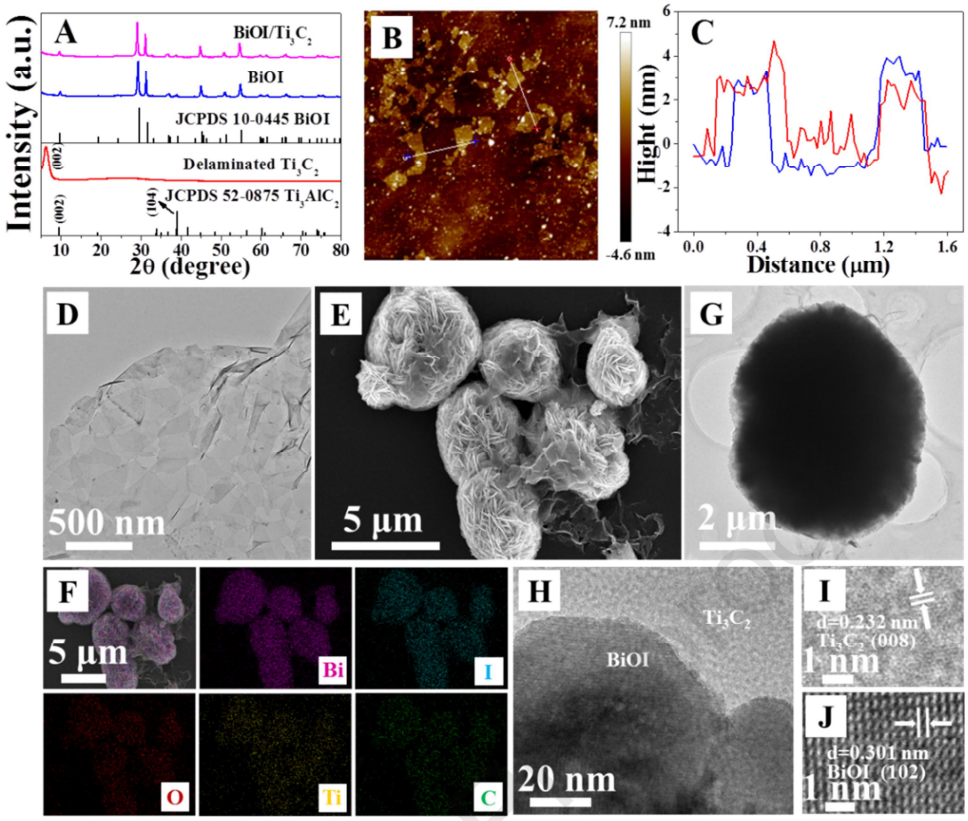

Fig. 1. (A) XRD patterns. (B) AFM image and (C) corresponding height profile of Ti_3C_2. (D) TEM image of Ti_3C_2. (E) SEM image and (F) the corresponding mapping images of BiOI/Ti_3C_2 heterostructure. (G, H) TEM and (I, J) HRTEM images of BiOI/Ti_3C_2 heterostructure.

3.1 Morphology and structure characterization of BiOI and BiOI/Ti_3C_2 heterostructure.

The crystal structure of the synthesized sample was analyzed by X-ray diffraction (XRD). As shown in Fig. 1A, after two-step treatments of the etching and delaminating, the typical diffraction peak assigned to Ti_3AlC_2 at 39° disappear, and the intense peak ascribed to the (002) crystal plane shifts from 9.4° to 6.3°, certifying the aluminum layer was successfully removed, and Ti_3AlC_2 has transformed to Ti_3C_2. In particular, the shift of (002) peak to lower angles indicates the intercalation of Li^+ among the layers of Ti_3C_2 [25]. Besides, the overall peaks located at 29.5°, 31.6°, 55.2° of BiOI are observed, which can be ascribed to tetragonal BiOI (JCPDS 10-0445). For BiOI/Ti_3C_2 heterostructure, the characteristic diffraction peaks exsit, and no diffraction peak of Ti_3C_2 is observed, which might be due to the low content and homogeneous dispersion of Ti_3C_2 in the heterostructure.

The morphology of the samples were studied by scanning electron microscope (SEM). Fig. S1A, B shows the SEM image of Ti_3AlC_2 and Ti_3C_2 nanosheets, respectively. As seen in Fig. 1B, atomic force microscopy (AFM) image shows the ultra thin foil, and the corresponding height profile displays the thickness of Ti_3C_2 nanosheets is about 3.2 nm (Fig. 1C), demonstrating the ultrathin structure of the Ti_3C_2 nanosheets. As seen in Fig. 1D, a thin 2D layered structure of Ti_3C_2 can be further observed from the transmission electron microscopy (TEM) image, especially because of the high atomic number of Ti [12]. As depicted in Fig. S1C, D, BiOI has a flower-like structure with an average grain size of 4 μm. Fig. 1E exhibits the SEM image of BiOI/Ti_3C_2 heterostructure, in which the flower-like BiOI was wrapped with Ti_3C_2 tightly. The corresponding energy-dispersive X-ray (EDX) spectroscopy mapping results confirm the presence and uniform distribution of Ti, C, Bi, O, and I (Fig. 1F). Moreover, the surface of the flower-like BiOI was covered with an ultrathin Ti_3C_2 nanosheet to form a 2D heterojunction (Fig. 1G and Fig. 1H). Fig. 1H-J exhibit the high-resolution TEM (HRTEM) images of BiOI/Ti_3C_2 heterostructure. Fig. 1I and Fig. 1J clearly shows the lattice spacing of 0.232 nm and 0.301 nm, which are attributed to the (008) crystal plane of Ti_3C_2 and the (102) crystal plane of BiOI, respectively. These results demonstrate the BiOI/Ti_3C_2 heterostructure with favourable interface interaction, which is beneficial to promote the separation of photogenerated carrier under light illumination, and thus acquire the satisfactory PEC response.

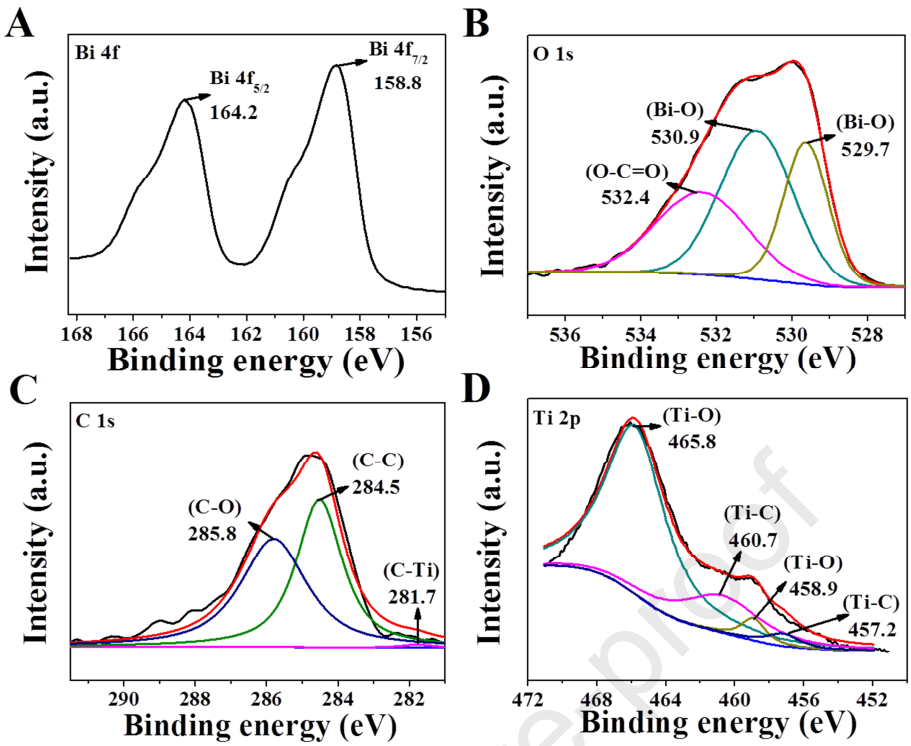

Fig. 2. High-resolution XPS spectra of BiOI/Ti_3C_2 heterostructure for (A) Bi 4f, (B) O 1s, (C) C 1s and (D) Ti 2p.

The surface chemical compositions and valence states of BiOI/Ti_3C_2 heterostructure were analyzed by X-ray photoelectron spectroscopy (XPS) spectra. The XPS survey spectrum (Fig. S2A) clearly certified the existence of all the elements of BiOI/Ti_3C_2 heterostructure, and the result is consistent with that of elemental mapping in Fig. 1F. Fig. 2A shows high resolution Bi 4f XPS spectrum. Two peaks located at 164.2 eV and 158.8 eV are separately ascribed to Bi $4f_{5/2}$ and Bi $4f_{7/2}$, which corresponds to Bi^{3+} of BiOI [26]. The peaks at binding energy of 529.7 eV and 530.9 are ascribed to the Bi-O bonds of BiOI, and the peak ascribed to 532.4 eV in BiOI/Ti_3C_2 heterostructure is assigned to O–C=O functional groups in Ti_3C_2 (Fig. 2B) [27]. As for I 3d spectrum (Fig. S2B), two peaks centered at 630.3 eV and 618.8 eV can be assigned to I $3d_{3/2}$ and I $3d_{5/2}$, respectively. In Fig. 2C, the spectrum of C 1s exhibits four typical peaks at 281.8, 284.5, 285.9 eV and 287.9 eV. In detail, the C 1s peak located at 284.5 eV belongs to the adventitious carbon (C-C), while the other three peaks at 281.7 eV and 285.8 eV are respectively assigned to C–Ti and C–O bonds [28]. For Ti 2p region, the peaks at 457.2 eV and 460.7 eV can be ascribed to

Ti–C bonds, and two peaks appeared at 458.9 eV and 465.8 eV attributed to Ti-O bonds (Fig. 2D). Noteworthily, the fact that the strongest peak located at 465.8 eV is assigned to Ti-O bonds, and the characteristic peak belonging to the Ti-F bonds cannot be observed powerfully demonstrates terminal –OH or –O substitute terminal –F. The result not only further confirms the strong interface interaction between BiOI and Ti_3C_2, but also indicates the massive possibility for Ti_3C_2 to capture photogenerated electrons from BiOI [29,30].

3.2. Electrochemical analysis of modified electrodes

Optical characterization of the prepared BiOI and BiOI/Ti_3C_2 heterostructure was researched using the UV-vis diffuse spectra. As can be seen in Fig. 3A, BiOI presents strong absorption in the visible light range. For BiOI/Ti_3C_2 heterostructure, an apparent red shift appears in comparison with BiOI, which benefits the augment of the visible light absorption. Furthermore, the Tauc plot is fitted, and then the band gap can be obtained according to the Tauc equation. As shown in Fig. 3A, the band gap energies (E_g) of BiOI and BiOI/Ti_3C_2 heterostructure are 1.9 eV and 1.7 eV, respectively. The corresponding conduction band (CB) and valence band (VB) can be calculated by following empirical formula [31]:

$$E_{CB} = \chi - E_0 - 0.5\,E_g, \quad (1)$$

$$E_{VB} = E_{CB} + E_g \quad (2)$$

Where E_{CB} and E_{VB} denote the conduction band (CB) and valence band (VB) edge potentials, respectively; χ represents the absolute electronegativity of the semiconductor, that is the geometric mean of the electronegativity, and the χ value of BiOI is 6.2 eV; E_0 indicates the energy of free electrons on the hydrogen scale (approximately 4.5 eV). And E_{CB} and E_{VB} of BiOI are calculated to be 0.85 eV and 2.75 eV. Besides, Fig. 3B shows the cathodic PEC response of the prepared photoelectrodes under visible light illumination. During the cathodic process, it is the photogenerated holes that is substantially determined for the cathodic photocurrent generation and augment. In the meanwhile, the oxygen dissolved in the electrolyte

acts as an acceptor to capture and consume the photogenerated electrons. Hence, the PEC tests were executed in an air-saturated electrolyte. The pure BiOI display a weaker photocurrent intensity (about 51 nA), while the BiOI/Ti_3C_2 heterostructure shows an enhanced photocurrent intensity (about 334 nA), which is six times as larger as that of BiOI, convincingly confirming the improvement of charge transfer ability of BiOI/Ti_3C_2 heterostructure with respect to pure BiOI. Additionally, the photocurrent intensity of Ti_3C_2 is extremely weak, verifying that the introduction of Ti_3C_2 is functioned to capture the photogenerated electron in BiOI/Ti_3C_2 heterostructure. Owing to its excellent electrical conductivity, Ti_3C_2 can promote photogenerated electrons transfer, greatly improving the photoelectric conversion efficiency of BiOI/Ti_3C_2 heterostructure.

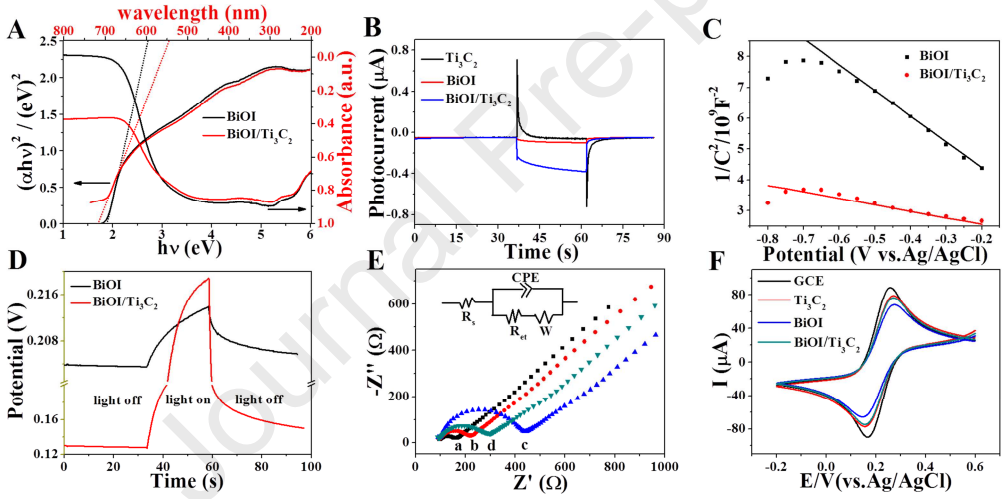

Fig. 3. (A) UV-vis diffuse reflectance spectra and Tauc's plots of the BiOI and BiOI/Ti_3C_2 heterostructure. (B) Photocurrent response for the designed sensor of Ti_3C_2/GCE, BiOI/GCE, and BiOI/Ti_3C_2/GCE. (C) Mott−Schottky plot of BiOI and BiOI/Ti_3C_2 heterostructure at 1 kHz under dark conditions. (D) OCP response of BiOI and BiOI/Ti_3C_2 heterostructure under dark and visible light irradiation. (E) EIS plots of (a) bare GCE, (b) Ti_3C_2/GCE, (c) BiOI/GCE, and (d) BiOI/Ti_3C_2/GCE in 0.1 M KCl solution containing 5.0 mM $[Fe(CN)_6]^{3-/4-}$ recorded in the frequency range from 0.1 Hz to 100 kHz. The inset shows the corresponding equivalent circuits. (F) CV curves of different electrodes in 0.1 M KCl solution containing 5.0 mM $[Fe(CN)_6]^{3-/4-}$.

Fig. 3C shows the Mott-Schottky (M-S) plots of BiOI and BiOI/Ti_3C_2 heterostructure, which can verdict the semiconductor type. The slope of linear part in M-S plots is positive for n-type semiconductor and negative for p-type semiconductor [32]. Obviously, the BiOI and the BiOI/Ti_3C_2 heterostructure display the properties of p-type semiconductor. Additionally, the carrier density is studied based on the slopes of the M-S plots *via* the following equation [33]:

$$N_d = (2/e\varepsilon\varepsilon_0)\,[d\,(1/C^2)/dV]^{-1}, \quad (3)$$

where e (e = 1.602 × 10^{-19} C) represents electronic charge unit, ε is the dielectric constant of material, ε_0 (ε_0 = 8.85 × 10^{-14} F cm^{-1}) is the permittivity of vacuum, and V denotes applied potential. As shown in Fig. 3C, the slope of BiOI/Ti_3C_2 heterostructure is much smaller compared to the pure BiOI, implying a higher carrier density that is closely relevant to the photocurrent intensity. Besides, we executed the open circuit potential (OCP) test to further investigate the property of BiOI/Ti_3C_2 heterostructure. Fig. 3D shows that OCP of the two samples dramatically shifts to much more positive potential with irradiation, and then slowly decreases without irradiation, indicating the effective hole transfer ability. Integrated the fact that the higher ΔOCP (OCP = OCP_{light} - OCP_{dark}) implied the larger band bending degree and the faster charge transfer at the electrode-electrolyte interface, BiOI/Ti_3C_2 heterostructure are confirmed to have better PEC activity [33,34].

Fig. 3E presents the electrochemical impedance spectroscopy (EIS) plots recorded on various electrodes, and the inset shows the corresponding equivalent circuits. The diameter of the semicircle in the high frequency region represents the charge transfer resistance (R_{ct}). Herein, the R_{ct} value for bare GCE is evaluated to be 90.09 Ω. After the electrode is modified with BiOI, the R_{ct} value is up to 331.7 Ω, while the R_{ct} value of BiOI/Ti_3C_2 heterostructure modified electrode decreased to be 225.8 Ω. This result indicates that Ti_3C_2 is beneficial to promote electron transfer and ensure better PEC performance for BiOI/Ti_3C_2 heterostructure. Furthermore, the Cyclic Voltammetry (CV) curves of various modified electrodes were determined in 1 M KCl solution containing 5.0 mM $[Fe(CN)_6]^{3-/4-}$ (Fig. 3F). The value of anode peak

current (i_p) for BiOI/GCE is 77.8 μA, lower than 102.5 μA of bare GCE. After modified with BiOI/Ti_3C_2 heterostructure, the i_p value increases to 87.4 μA. The increase is due to the good conductivity of Ti_3C_2, which improves the surface activity of the electrode and leads to an increase in peak current.

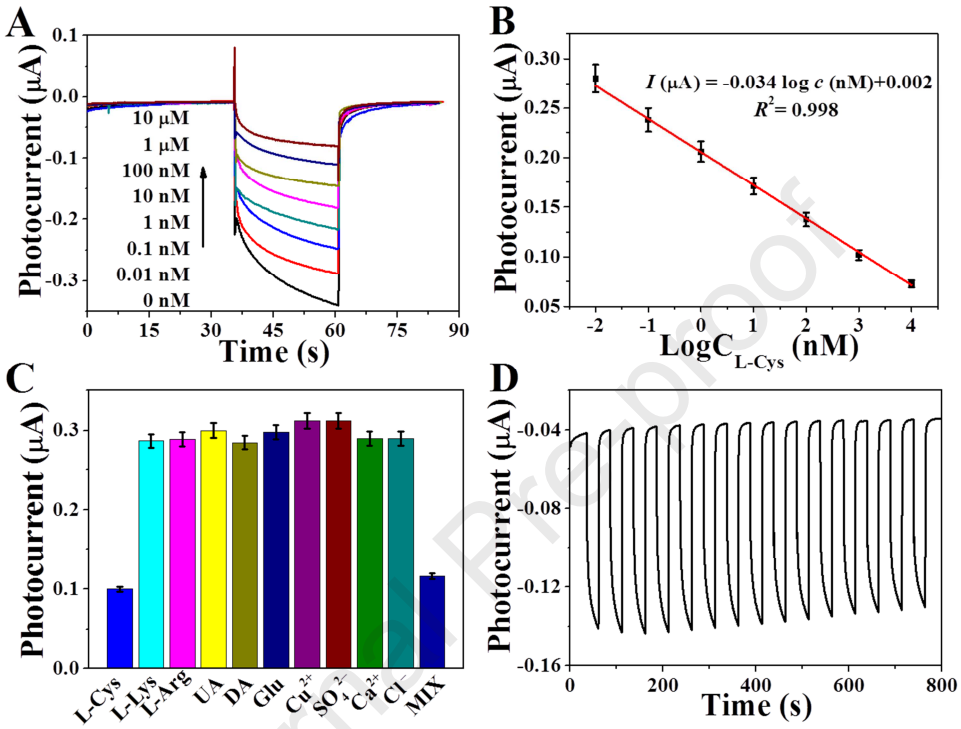

Fig. 4. (A) PEC responses of the fabricated sensor in 0.1 M phosphate buffer containing 0, 0.01, 0.1, 1, 10, 100, 1000 and 10000 nM L-Cys at -0.2 V. (B) The corresponding calibration curve for the determination of L-Cys. (C) The evaluation of specificity of the proposed PEC sensor to the interfering substances (photocurrent intensity of 1 μM L-Cys, 10 μM L-Lys, 10 μM L-Arg, 10 μM UA, 10 μM DA, 10 μM Glu, 10 μM Cu^{2+},10 μM SO_4^{2-},10 μM Ca^{2+} and 20 μM Cl^- in 0.1 M phosphate buffer). (D) Stability of PEC sensor in 0.1 M phosphate buffer containing 1 μM L-Cys.

3.3. Optimization of experimental conditions.

To obtain a better PEC performance, the influences of concentration of $BiOI/Ti_3C_2$ heterostructure, pH value of phosphate buffer and incubation time of target during PEC detection toward L-Cys is studied. As shown in Fig. S3A, the photocurrent intensity increases with a concentration increase of $BiOI/Ti_3C_2$ heterostructure from 0.5 to 2 mg mL^{-1}. Since the further augment of $BiOI/Ti_3C_2$ heterostructure, the photocurrent intensity decreases slightly, probably due to the thicker coating hindering electron transfer. Moreover, the incubation time of L-Cys has a significant effect on the performance of the PEC sensor. As can be seen in Fig. S3B, with the extension of incubation time, the photocurrent intensity decreases rapidly up and then levels off after 30 min. Hence, 2 mg mL^{-1} for the optimal concentration of $BiOI/Ti_3C_2$ heterostructure and 30 min for the optimal incubation time of L-Cys are applied for further experiment.

3.4. Photoelectrochemical sensing of L-Cys.

Under the optimal experimental conditions, the proposed PEC biosensor was applied to the quantitative determination of L-Cys. Fig. 4A displays the relationship between the concentration of L-Cys and photocurrent intensity. The larger the concentration of L-Cys, the weaker the photocurrent intensity. The results may be caused by the steric hindrance effect, inducing the photocurrent response decreases spontaneously for the established PEC platform. Moreover, the photocurrent intensity is well linear to the logarithm of L-Cys concentration in the range from 0.01 nM to 10 μM (Fig. 4B). The corresponding linear regression equation is I (μA) = -0.034 log c (nM) + 0.002 (correlation coefficient R^2 = 0.998). Besides, the limit of detection (LOD) is estimated to be 0.005 nM based on the analytical function of LOD=Kσ/S, where K is used as 3, σ is the standard deviation of the blank solution (n=10), S is the slope of regression line. Compared with the various method for L-Cys determination reported in the previous reports (Table S1), the proposed PEC sensor shows a wider linear range and lower detection limit.

3.5. Selectivity, stability and reproducibility of the PEC sensor.

Since the selectivity is a vital factor for the PEC performance of proposed biosensor, interference measurement was carried out by evaluating the PEC response (1 μM L-Cys, 10 μM L-Lys, 10 μM L-Arg, 10 μM UA, 10 μM DA, 10 μM Glu, 10 μM Cu^{2+},10 μM SO_4^{2-},10 μM Ca^{2+} and 20 μM Cl^- in 0.1 M phosphate buffer). As shown in Fig. 4C, the PEC response signal has almost no change before and after the existence of above mentioned interferences instead of the target. The photocurrent intensity decreases in the case of target existing or target and potential interferences coexisting, since only the group of –SH in the structure of L-Cys can forcefully and effectively interact with the surface of the modified photoelectrode. The results indicate that the proposed PEC platform possesses good selectivity towards L-Cys sensing. By the way, as far as we know that L-Cys detection is prone to be affected by the possible oxidation reactions happened in the interface of PEC platform, the proposed PEC biosensor on the basis of the cathodic photocurrent signal can skillfully evade the issue, and then achieve more accurate PEC performance. Moreover, the stability of the PEC biosensor was studied. Fig. 4D shows the photocurrent intensity of prepared photoelectrode containing 1 μM L-Cys. After 15 times testing based on the off-on irradiation cycle, the photocurrent intensity remained 95% of the initial one, which shows accredited stability. Besides, the reproducibility of the sensor was also examined *via* contrasting six individual modified photoelectrodes. As depicted in Fig. S4, a relative standard deviation (RSD) of 3.4% was obtained, indicating good reproducibility of the proposed PEC sensing platform.

4. Conclusion

In summary, BiOI/Ti_3C_2 heterostructure has been successfully synthesized, and applied to PEC analysis. Highly sensitive, stability and selective L-Cys monitoring was achieved *via* BiOI/Ti_3C_2 heterostructure serving as a photocathode. Considering the Schottky junction-based PEC sensing platform, we demonstrate that the combined merits of proposed photocathode of built-in electric field generation and contact

resistance diminution can efficiently boost the PEC performance with "signal-off" pattern. Given those unique properties, the LOD of L-Cys sensing based on the PEC analytic technique is as low as 0.005 nM. The study unveils the immense potential of Ti_3C_2 MXene-based photoactive heterostructure in the establishment of PEC sensing platform, and paves the road for application in photocatalysis and PEC sensor.

CRediT authorship contribution statement

Cui Ye: Writing-review &editing, funding acquisition, supervision. **Zhen Wu, Keyi Ma and Zhuohao Xia:** Writing-original draft, data curation. **Jun Pan:** Formal analysis. **Minqiang Wang:** Writing-review & editing, formal analysis. **Changhui Ye:** Funding acquisition.

Declaration of Competing Interest

The authors declare that they have no known competing financial interests or personal relationships that could have appeared to influence the work reported in this paper.

Appendix A. Supplementary data

Supplementary information related to this article can be found in the online version.

Acknowledgement

This work was supported by the National Natural Science Foundation of China (Grant No. 21904116). The authors are grateful to Prof. Changhui Ye (Deceased on Nov 1 2019) for assistance.

References

[1] C. Ye, M. Q. Wang, H. Q. Luo, N. B. Li, Label-free Photoelectrochemical "Off−On" Platform Coupled with G-wire-enhanced Strategy for Highly Sensitive MicroRNA Sensing in Cancer Cells, Anal. Chem. 89 (2017) 11697–11702.

[2] Y. T. Long, C. Kong, D. W. Li, Y. Li, S. Chowdhury, H. Tian, Ultrasensitive Determination of Cysteine Based on the Photocurrent of Nafion-functionalized CdS–MV Quantum Dots on an

ITO Electrode, Small 7 (2011) 1624–1628.

[3] R. Zeng, L. Zhang, L. Su, Z. Luo, Q. Zhou, D. Tang, Photoelectrochemical Bioanalysis of Antibiotics on rGO-Bi_2WO_6-Au Based on Branched Hybridization Chain Reaction, Biosens. Bioelectron. 133 **(**2019) 100–106.

[4] C. Ye, M. Q. Wang, L. J. Li, H. Q. Luo, N. B. Li, Fabrication of Pt/$Cu_3(PO_4)_2$ Ultrathin Nanosheet Heterostructure for Photoelectrochemical MicroRNA Sensing Using Novel G-wire-enhanced Strategy, Nanoscale 9 (2017) 7526–7532.

[5] C. Ye, M. Q. Wang, Z. F. Gao, Y. Zhang, J. L. Lei, H. Q. Luo, N. B. Li, Ligating Dopamine as Signal Trigger onto the Substrate via Metal-catalyst-free Click Chemistry for "Signal-On" Photoelectrochemical Sensing of Ultralow MicroRNA Levels, Anal. Chem. 88 (2016) 11444−11449.

[6] Z. F. Gao, R. Liu, J. Wang, J. Dai, W. H. Huang, M. Liu, S. Wang, F. Xia, S. Zhang, L. Jiang , Manipulating the Hydrophobicity of DNA as a Universal Strategy for Visual Biosensing, Nat. Protoc. 15 (2020) 316–337.

[7] L. M. Yu, Y. C. Zhu, Y. L. Liu, P. Qu, M. T. Xu, Q. Shen, W. W. Zhao, Ferroelectric Perovskite Oxide@TiO_2 Nanorod Heterostructures: Preparation, Characterization, and Application as a Platform for Photoelectrochemical Bioanalysis, Anal. Chem. 90 (2018) 10803−10811.

[8] R. Xu, Y. Jiang, L. Xia, T. Zhang, L. Xu, S. Zhang, D. Liu, H. Song, A Sensitive Photoelectrochemical Biosensor for AFP Detection Based on ZnO Inverse Opal Electrodes with Signal Amplification of CdS-QDs, Biosens. Bioelectron. 74 (2015) 411–417.

[9] Y. Zang, J. Lei, Q. Hao, H. Ju, CdS/MoS_2 Heterojunction-based Photoelectrochemical DNA Biosensor via Enhanced Chemiluminescence Excitation, Biosens. Bioelectron. 77 (2016) 557–564.

[10] L. Tang, X. Ouyang, B. Peng, G. Zeng, Y. Zhu, J. Yu, C. Feng, S. Fang, X. Zhu, J. Tan, Highly Sensitive Detection of Microcystin-LR under Visible Light Using a Self-powered Photoelectrochemical Aptasensor Based on a CoO/Au/g-C_3N_4 Z-scheme Heterojunction, Nanoscale 11 (2019) 12198–12209.

[11] M. Naguib, M. Kurtoglu, V. Presser, J. Lu, J. Niu, M. Heon, L. Hultman, Y. Gogotsi, M. W. Barsoum, Two-Dimensional Nanocrystals Produced by Exfoliation of Ti_3AlC_2, Adv. Mater. 23 (2011) 4248–4253.

[12] W. Yuan, L. Cheng, Y. An, H. Wu, N. Yao, X. Fan, X. Guo, MXene Nanofibers as Highly Active Catalysts for Hydrogen Evolution Reaction, ACS Sustain. Chem. Eng. 6 (2018) 8976−8982.

[13] C. Chen, X. Xie, B. Anasori, A. Sarycheva, T. Makaryan, M. Zhao, P. Urbankowski, L. Miao, J. Jiang, Y. Gogotsi, MoS_2-on-MXene Heterostructures as Highly Reversible Anode Materials for Lithium-Ion Batteries, Angew. Chem., Int. Ed. 57 (2018) 1846–1850.

[14] H. Wang, H. Li, Y. Huang, M. Xiong, F. Wang, C. Li, A Label-free Electrochemical Biosensor for Highly Sensitive Detection of Gliotoxin Based on DNA Nanostructure/MXene Nanocomplexes, Biosens. Bioelectron. 142 (2019) 111531.

[15] L. Bi, Z. Yang, L. Chen, Z. Wu, C. Ye, Compressible AgNWs/$Ti_3C_2T_x$ MXene Aerogelbased Highly Sensitive Piezoresistive Pressure Sensor as Versatile Electronic Skins, J. Mater. Chem. A, 8 (2020) 20030.

[16] C. Peng, X. Yang, Y. Li, H. Yu, H. Wang, F. Peng, Hybrids of Two-Dimensional Ti_3C_2 and TiO_2 Exposing {001} Facets toward Enhanced Photocatalytic Activity, ACS Appl. Mater. Interfaces 8 (2016) 6051−6060.

[17] Z. Kang, Y. Ma, X. Tan, M. Zhu, Z. Zheng, N. Liu, L. Li, Z. Zou, X. Jiang, T. Zhai, Y. Gao, MXene–Silicon Van Der Waals Heterostructures for High-speed Self-driven Photodetectors，Adv. Electron. Mater. 3 (2017) 1700165.

[18] H. Wang, C. Si, J. Zhou, Z. Sun, Vanishing Schottky Barriers in Blue Phosphorene/MXene Heterojunctions, J. Phys. Chem. C 121 (2017) 25164–25171.

[19] Y. Zhu, X. Liu, K. Yan, J. Zhang, A Cathodic Photovoltammetric Sensor for Chloramphenicol Based on BiOI and Graphene Nanocomposites, Sens. Actuators B Chem. 284 (2019) 505–513.

[20] Y. Zhu, K. Yan, Z. Xu, J. Wu, J. Zhang, Cathodic “signal-on” Photoelectrochemical Aptasensor for Chloramphenicol Detection Using Hierarchical Porous Flower-like Bi-BiOI@C Composite, Biosens. Bioelectron. 131 (2019) 79−87.

[21] N. I. Ismail, Y. Z. H. Y. Hashim, P. Jamal, R. Othman, H. M. Salleh, Production of Cysteine: Approaches, Challenges and Potential Solution, Int. J. Biotech. Well. Indus. 3 (2014) 95−101.

[22] Y. Zhu, Z. Xu, K. Yan, H. Zhao, J. Zhang, One-Step Synthesis of CuO−Cu_2O Heterojunction by Flame Spray Pyrolysis for Cathodic Photoelectrochemical Sensing of L-Cysteine, ACS Appl. Mater. Interfaces 9 (2017) 40452−40460.

[23] S. Shahrokhian, Lead Phthalocyanine as a Selective Carrier for Preparation of a Cysteine-selective Electrode, Anal. Chem. 73 (2001) 5972−5978.

[24] J. A. Rodriguez, J. Dvorak, T. Jirsak, G. Liu, J. Hrbek, Y. Aray, C. González, Coverage Effects and the Nature of the Metal-Sulfur Bond in S/Au (111): High-Resolution Photoemission and Density-functional Studies, J. Am. Chem. Soc. 125 (2003) 276-285.

[25] M. Alhabeb, K. Maleski, B. Anasori, P. Lelyukh, L. Clark, S. Sin, Y. Gogotsi, Guidelines for Synthesis and Processing of Two-Dimensional Titanium Carbide (Ti_3C_2Tx MXene), Chem. Mater. 29 (2017) 7633−7644.

[26] H. Wang, H. Ye, B. Zhang, F. Zhao, B. Zeng, Electrostatic Interaction Mechanism Based Synthesis of a Z-scheme BiOI–CdS Photocatalyst for Selective and Sensitive Detection of Cu^{2+}, J. Mater. Chem. A, 5 (2017) 10599−10608.

[27] H. Wang, Y. Liang, L. Liu, J. Hu, P. Wu, W. Cui, Enriched Photoelectrocatalytic Degradation and Photoelectric Performance of BiOI Photoelectrode by Coupling rGO, Appl. Catal. B. 208 (2017) 22–34.

[28] S. Cao, B. Shen, T. Tong, J. Fu, J. Yu, 2D/2D Heterojunction of Ultrathin MXene/Bi_2WO_6 Nanosheets for Improved Photocatalytic CO_2 Reduction, Adv. Funct. Mater. 28 (2018) 1800136.

[29] J. Ran, G. Gao, F. T. Li, T. Y. Ma, A. Du, S. Z. Qiao, Ti_3C_2 MXene Co-catalyst on Metal Sulfide Photo-absorbers for Enhanced Visible-light Photocatalytic Hydrogen Production, Nat. Commun. 8 (2017) 13907.

[30] J. Ke, J. Liu, H. Sun, H. Zhang, X. Duan, P. Liang, X. Li, M. Q. Tade, S. Liu, S. Wang, Facile Assembly of Bi_2O_3/Bi_2S_3/MoS_2 n-p Heterojunction with Layered n-Bi_2O_3 and p-MoS_2 for Enhanced Photocatalytic Water Oxidation and Pollutant Degradation, Appl. Catal. B. 200 (2017) 47–55.

[31] D. Jiang, X. Du, D. Chen, Y. Li, N. Hao, J. Qian, H. Zhong, T. You, K. Wang, Facile Wet Chemical Method for Fabricating p-Type BiOBr/n-Type Nitrogen Doped Graphene Composites: Efficient Visible-excited Charge Separation, and High-performance Photoelectrochemical Sensing, Carbon 102 (2016) 10–17.

[32] A. Ali, F. A. Mangrio, X. Chen, Y. Dai, K. Chen, X. Xu, R. Xia, L. Zhu, Ultrathin MoS_2 Nanosheets for High-performance Photoelectrochemical Applications via Plasmonic Coupling with Au Nanocrystals, Nanoscale 11 (2019) 7813–7824.

[33] Q. Wang, H. Zhu, B. Li, Synergy of Ti-O-based Heterojunction and Hierarchical 1D Nanobelt/3D Microflower Heteroarchitectures for Enhanced Photocatalytic Tetracycline Degradation and Photoelectrochemical Water Splitting, Chem. Eng. J. 378 (2019) 122072.

[34] J. Li, X. Gao, B. Liu, Q. Feng, X. B. Li, M. Y. Huang, Z. Liu, J. Zhang, C. H. Tung, L. Z. Wu, Graphdiyne: A Metal-free Material as Hole Transfer Layer To Fabricate Quantum Dot-sensitized Photocathodes for Hydrogen Production, J. Am. Chem. Soc. 138 (2016) 3954− 3957.

- Schottky junction-based $BiOI/Ti_3C_2$ heterostructure was applied as a photocathode for photoelectrochemical (PEC) bioanalysis
- $BiOI/Ti_3C_2$ heterostructure possesses admirably combined merits, noting in particular the generation of built-in electric field and the decrease of contact resistance between BiOI and Ti_3C_2.
- The proposed PEC sensing platform shows excellent performance in terms of sensitivity, limit of detection (LOD, 0.005 nM) and stability for L-Cys monitoring.
- This work demonstrates Ti_3C_2 MXene-based Schottky heterostructure for the establishment of PEC biosensor.

Declaration of interests

☒ The authors declare that they have no known competing financial interests or personal relationships that could have appeared to influence the work reported in this paper.

☐The authors declare the following financial interests/personal relationships which may be considered as potential competing interests:

Credit Author Statement

Cui Ye: Writing-review &editing, funding acquisition, supervision. **Zhen Wu, Keyi Ma and Zhuohao Xia:** Writing-original draft, data curation. **Jun Pan:** Formal analysis. **Minqiang Wang:** Writing-review & editing, formal analysis. **Changhui Ye:** Funding acquisition.